Research

Author for correspondence:
F. Barthelat
e-mail: francois.barthelat@mcgill.ca

The quest for stiff, strong and tough hybrid materials: an exhaustive exploration

F. Barthelat and M. Mirkhalaf

Department of Mechanical Engineering, McGill University, 817 Sherbrooke Street West, Montreal, Quebec, Canada H3A 2K6

How to arrange soft materials with strong but brittle reinforcements to achieve attractive combinations of stiffness, strength and toughness is an ongoing and fascinating question in engineering and biological materials science. Recent advances in topology optimization and bioinspiration have brought interesting answers to this question, but they provide only small windows into the vast design space associated with this problem. Here, we take a more global approach in which we assess the mechanical performance of thousands of possible microstructures. This exhaustive exploration gives a global picture of structure–property relationships and guarantees that global optima can be found. Landscapes of optimum solutions for different combinations of desired properties can also be created, revealing the robustness of each of the solutions. Interestingly, while some of the major hybrid designs used in engineering are absent from the set of solutions, the microstructures emerging from this process are reminiscent of materials, such as bone, nacre or spider silk.

1. Introduction

Hybrid materials combine at least two components with complementary properties, generating attractive combinations of performance and functionality which are inaccessible to monolithic materials [1]. In terms of design, hybrid materials offer a rich and vast playground: properties can be tuned by manipulating the individual components, their volumetric content, their morphology, their size and arrangement [2]. How to tune these parameters for optimum performance represents a fascinating and highly relevant problem in materials science [3,4]. However, despite the vast number of possibilities, only a handful of designs currently dominate the engineering world: fibre reinforced composites, laminates, cellular materials and solid foams. Much research and development have been devoted to optimizing these particular morphologies [5–7] following the optimization approach depicted in figure 1a, in which a set of desired properties is selected and the optimization procedure proceeds, by successive alterations of the microstructure, towards that objective. More recently, topology optimization methods led to interesting new designs and classes of hybrid materials [5,8–16]. However, these optimization approaches are not always robust, and the design space and type of microstructure must be restricted to facilitate convergence. The result may also 'fall' into local optima, occluding potentially interesting designs [17,18]. Another possible approach is the so-called 'exhaustive search' or 'brute force' optimization. In this approach, all possible designs are assessed without the need to pre-determine a set of desired properties (figure 1b). This approach, while in principle simple, is traditionally deemed inappropriate because of the large number of combinations which must be evaluated. Recently, the validity of this approach has however been re-evaluated in the light of today's raw computational power and parallel processing [19]. An exhaustive exploration not only guarantees that the global optimum structure for a range of desired properties can be found, it also provides a comprehensive picture of the entire design space and unique insights into structure–property relationships.
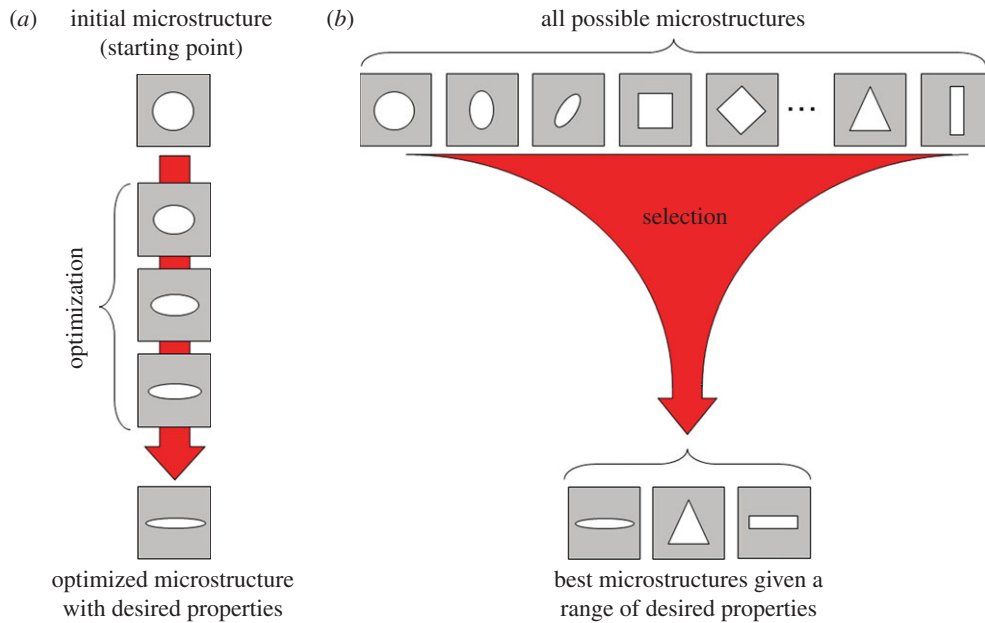
Figure 1. (a) A typical microstructure optimization. A topology is selected and its morphology is optimized for a pre-defined set of desired properties and (b) in the exhaustive approach, all possible microstructures are explored. The best microstructures can be easily selected for a given set of properties or range of properties. (Online version in colour.)

Here, we focus on the problem of how to combine a soft, energy dissipating material with a stiff and strong, but brittle material. This combination is common in engineering composites (carbon fibre reinforced polymers) and in biological composites (nacre, bone, tooth enamel, fish scales and arthropod cuticles [20–24]). The soft phase typically provides energy dissipation, toughness and ductility, whereas the hard phase provides stiffness. The unique combinations of properties they offer make hard–soft hybrid materials suitable for a variety of functions: structural support, protection, absorption of impact energy. The pathway towards achieving these functions raises interesting questions for both engineering and biological materials: how much of the hard phase should be incorporated and under which form? Large volume fractions of hard materials lead to high modulus and hardness as seen in tooth enamel or urchin spicules. However, with these improvements comes brittleness, the price to pay for high stiffness and strength [4]. Can the microstructure offset this brittleness as seen in some biological materials? Are there other efficient ways to arrange hard and soft which are neither used in engineering nor observed in nature? In this work, we set up an exhaustive search as an attempt to formally explore these broad questions.

2. Microstructural models

To explore these questions, we set up a model to predict the mechanical response of hybrids of hard and soft materials. The model had to give enough flexibility to explore the responses of a large number of combinations of volume fractions and morphologies. At the same time, computational cost had to be kept low so that evaluating the performance of thousands of microstructures became feasible. We therefore developed a simple finite-element model that did not necessarily capture the exact material response in terms of stresses and strains, but which could serve as a basis to compare and identify the best microstructures for desired sets of properties. We considered two-dimensional microstructures with periodicity along two perpendicular directions (figure 2a). The aim

is to predict the stress–strain response of this microstructure when it is stretched along the horizontal direction. Figure 2b shows a 'unit cell' which is representative of the microstructure, also called representative volume element (RVE). Appropriate periodic boundary conditions must be enforced on the boundary of the model

$$
\left.
\begin{aligned}
u_x(\alpha, y) - u_x(-\alpha, y) &= u_x(\alpha, 0) - u_x(-\alpha, 0), \\
u_y(\alpha, y) &= u_y(-\alpha, y), \\
u_x(x, 1) &= u_x(x, -1)
\end{aligned}
\right\}
$$
$$
\text{and} \quad u_y(x, 1) - u_y(x, -1) = u_y(0, 1) - u_y(0, -1). \quad (2.1)
$$

We also assumed symmetries about the x- and y-axes, so that only a quarter of the element was actually modelled (figure 2c). With this assumption, the displacement must also be symmetric

$$
\left.
\begin{aligned}
u_x(-x, y) &= -u_x(x, y), \\
u_y(-x, y) &= u_y(x, y), \\
u_x(x, -y) &= u_x(x, y)
\end{aligned}
\right\}
$$
$$
\text{and} \quad u_y(x, -y) = -u_y(x, y). \quad (2.2)
$$

Combining (2.1) and (2.2) leads to the periodic-symmetric boundary conditions [25]

$$
\left.
\begin{aligned}
u_x(0, y) &= 0, \\
u_x(\alpha, y) &= u_x(\alpha, 1), \\
u_y(x, 0) &= 0
\end{aligned}
\right\}
$$
$$
\text{and} \quad u_y(x, 1) = u_y(\alpha, 1). \quad (2.3)
$$

These equations were implemented using multi-point constraints. To simulate uniaxial tension along the x-axis, the overall strain along the x-axis was progressively increased, by specifying the displacement $u_x(\alpha, 1) = \alpha \varepsilon$ at the upper right corner of the model (figure 2c). The model was free to contract in the transverse direction from Poisson's effects. The model was divided into nine cells, each of which could be made of either soft or hard material. The total number of possible arrangements for soft and hard was therefore $2^9 = 512$. Some of these configurations were, however,
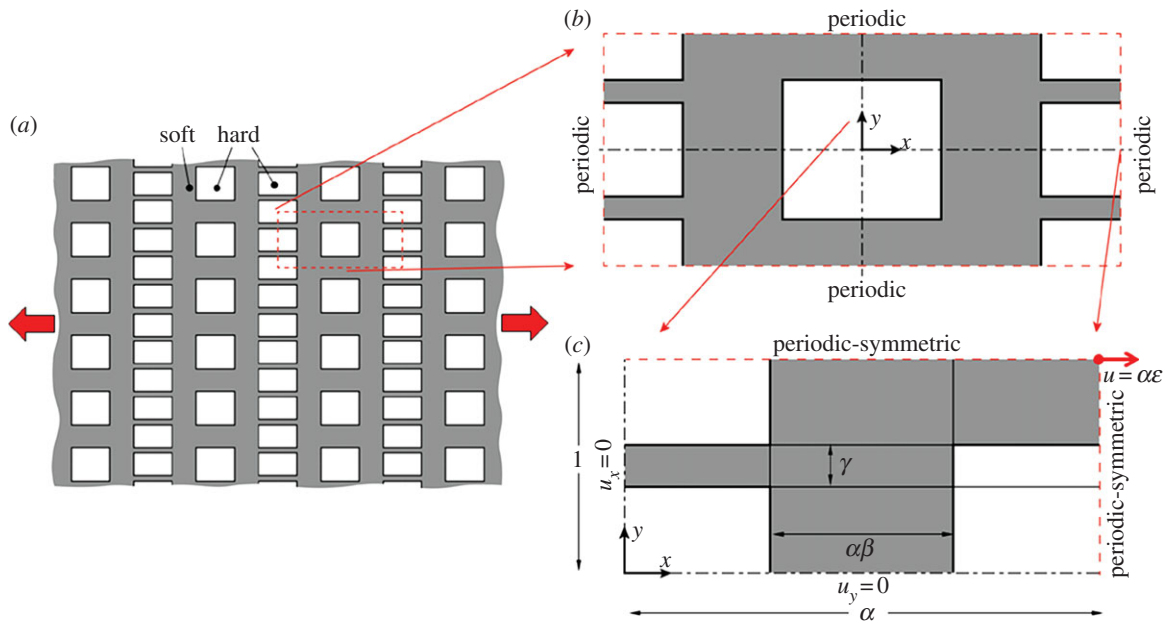
Figure 2. (*a*) A two-dimensional microstructure with periodicity along two perpendicular directions. The material is stretched along the horizontal direction. (*b*) Schematic of an RVE representation of the microstructure. Periodic boundary conditions are applied (*c*): using symmetries only a quarter of the RVE is modelled, using periodic-symmetric conditions. (Online version in colour.)

redundant after applying symmetries and periodicity. Also, configurations where the patches of hard phase joined at only one corner were deemed unrealistic and excluded using a connectivity check algorithm. After removing the redundant and forbidden configurations, 112 possible configurations remained. The morphology was also further adjusted through three non-dimensional parameters α, β and γ, which controlled the aspect ratio of the RVE, as well as the internal morphology of the cells (figure 2*c*). The height of the model was set to one, because no size effect was considered in the model. Four values were considered for each of these parameters: $\alpha = 1, 2, 5, 10$; $\beta = 0.1, 0.2, 0.5, 0.9$ and $\gamma = 0.1, 0.2, 0.5, 0.9$. These values were selected in order to capture the widest possible range of morphologies and mechanical responses.

There are $4^3 = 64$ combinations of α, β and γ for each of the 112 distributions for soft and hard phases, yielding a total number of 7168 models. Each of the cells was meshed with plane strain elements, with material properties corresponding to either the soft or the hard phase. The mesh was refined until the response of the microstructures with respect to one another was not affected by further mesh refinements. The hard phase was modelled as linear elastic with modulus $E_h = 100$ GPa and tensile strength $\sigma_h = 100$ MPa; its Poisson's ratio was kept at a constant value of 0.2, typical of a ceramic [26]. The failure of the hard phase was modelled as brittle, and a failure criterion based on maximum tensile stress was therefore used (material fails when $\sigma_{max} = \sigma_h$). The energy dissipated upon failure of the hard phase was assumed to be negligible compared with other dissipative processes in the soft phase. The soft phase was modelled as linear elastic–perfectly plastic with modulus $E_s = 1$ GPa and yield strength $\sigma_s = 1$ MPa; its Poisson's ratio was kept at a constant value of 0.4, typical of a polymer [27]. The polymer yielded following a Drucker–Prager yield criterion [28,29] in order to capture the formation of cavitation bubbles and ligaments typical of biological and synthetic polymers undergoing tensile deformations. In this

model, the yield strength of the soft phase decreases when the mean stress increases, following:

$$\frac{(3 - \sin \varphi)}{6} \sqrt{3 J_2} = c \cos \varphi - \sin \varphi \sigma_m, \tag{2.4}$$

where J_2 is the second invariant of the deviator part of the Cauchy stress, σ_m is the mean stress, c and ϕ are two material properties corresponding to cohesion and friction angle, respectively. For the simulations, we used $c = 0.793$ MPa and $\varphi = 40°$, corresponding to a yield strength of $\sigma_s = 1$ MPa in uniaxial tension [28]. In the post yield regime, the soft material was assumed to be perfectly plastic, with an associated flow rule capturing the volumetric expansion of the material consistent with cavitation and the formation of ligaments. Failure of the soft phase was governed by a strain-based criterion where the material completely fails when the equivalent strain reaches $\varepsilon_s = 0.1$, corresponding to the strain at failure of the soft phase in uniaxial tension. This set of material properties was chosen to create a strong contrast of properties between the hard and soft phases: $E_h/E_s = 100$, $\sigma_h/\sigma_s = 100$ and $\varepsilon_h/\varepsilon_s = 0.01$. A set of models with lower contrast ($E_h/E_s = 10$, $\sigma_h/\sigma_s = 10$ and $\varepsilon_h/\varepsilon_s = 0.01$) was also generated. Macroscopic stresses and strains were computed from the imposed displacement and the reaction force along the x-direction (as expected, the reaction force along the y-direction was zero for all the models). Failure criteria for hard and soft components were then applied to determine at which stress and strain the hybrid material failed. We automated the entire process of model generation and analysis with a combination of MATLAB (R2012a, MA, USA) and ANSYS (v. 9, PA, USA).

3. Results

Figure 3*a* shows a set of 7168 tensile stress–strain curves resulting from this exhaustive exploration, and for the case of a high contrast of properties between hard and soft phases: $E_h/E_s = 100$, $\sigma_h/\sigma_s = 100$ and strain at failure $\varepsilon_h/\varepsilon_s = 0.01$.
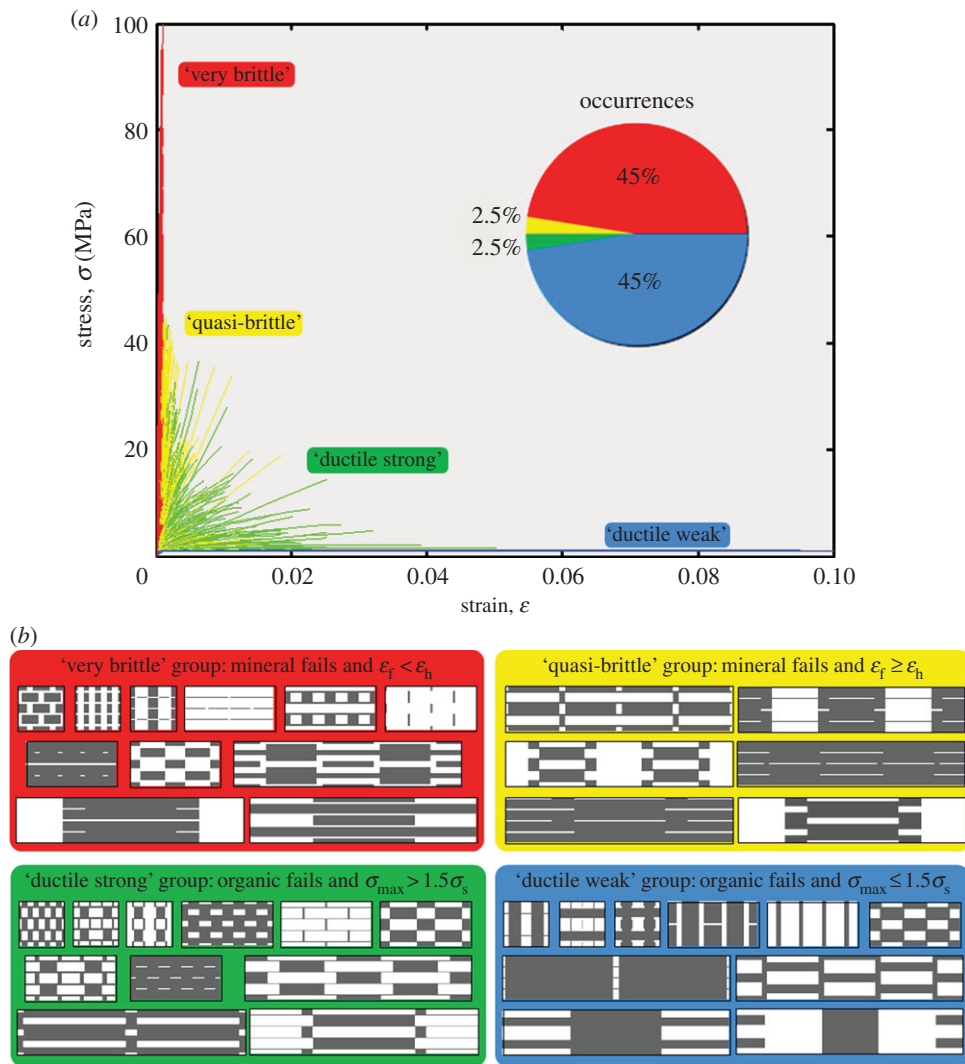
Figure 3. (*a*) Tensile stress–strain curves for 7168 microstructures. The mechanical properties fall into four groups and (*b*) examples of microstructures from each of these groups. (Online version in colour.)

The exploration produced a wide range of responses ranging from brittle to ductile, the majority of them being close, in behaviour, to either the hard phase (very brittle) or the soft phase (very soft). About half of the models failed by ductile failure of the soft phase, while the other half failed by brittle failure of the hard phase. Upon closer inspection, we classified the microstructures into four groups according to their mechanical response (figure 3*b*). The 'very brittle' group, representing about 45% of all structures produced, failed at strains smaller than the strain at failure of the hard phase, with negligible energy dissipation. This group included microstructures with a wide range of compositions, but where all or part of the hard phase was continuous along the direction of loading (figure 3*b*). In this configuration, most of the stresses were channelled through the hard phase, which produced a stiff but brittle behaviour. Stress concentrations in the hard phase reduced the strain at failure to values smaller than pure hard phase. Less than 2.5% of the models failed by fracture of the hard phase, but at strains larger (up to 20 times larger) than the failure strain of the hard phase. This second group, which we called 'quasi-brittle', therefore dissipated more energy. The materials in this group displayed a discontinuous hard phase with high aspect ratio (figure 3*b*). This arrangement led to a configuration where the matrix imposed shear stresses on the inclusions, while the hard inclusions were subjected to tension. While significant yielding of the matrix was observed in

this group, the aspect ratio of the hard phase was high enough to fail the hard phase. The next two groups failed by ductile failure of the soft phase.

About 45% of the models displayed low strength, not greater than one and a half times the strength of the soft phase. We therefore termed this third group as 'ductile weak' (figure 3*b*). This group included microstructures with a wide range of compositions but with one common trait: the materials contained straight, uninterrupted bands of the soft phase across the direction of loading. As a result of this arrangement, the improvement in strength was minimal, and energy dissipation and strain at failure were not always large. Finally, failure of about 2.5% of the materials was controlled by failure of the soft phase, but at strengths greater than one and half times the strength of the soft material. This fourth 'strong ductile' group (figure 3*b*) was stronger than group three, because it contained structures where the soft phase formed continuous but jagged bands across the direction of loading. The staggered structure, found in a large variety of natural materials such as bone and nacre, was a part of this group.

To further the analysis, we extracted three key properties from each of the stress–strain curves: elastic modulus E (i.e. stiffness: initial slope of the stress–strain curve), strength σ (maximum tensile stress that the material can sustain) and energy absorption to failure U (mechanical energy dissipated
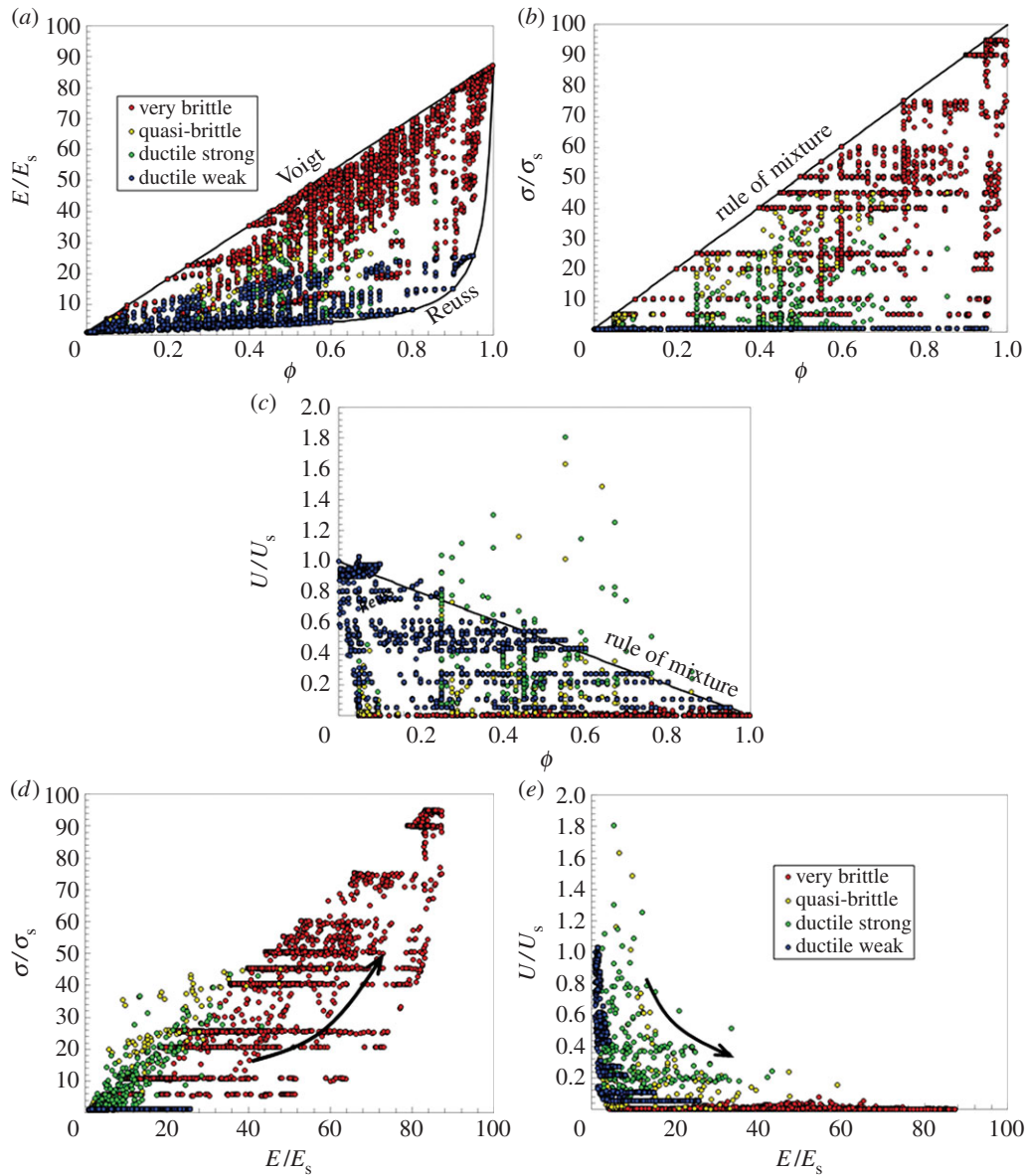
Figure 4. Normalized properties as functions of the concentration of hard phase: (*a*) modulus, (*b*) strength, (*c*) energy, (*d*) strength versus modulus and (*e*) energy absorption versus modulus. (Online version in colour.)

by the material before failure). Energy dissipation was measured by calculating the area under the stress–strain curve up to failure, and subtracting the elastic energy which would be recovered upon unloading just prior to failure. With this definition, pure hard phase had zero energy absorption (the amount of energy absorbed by the generation of new surfaces in the brittle fracture process was neglected). E, σ and U were normalized by the properties of the soft material in order to highlight the effect of incorporating a hard phase into a soft matrix, and the normalized properties were then plotted as functions of the concentration of the hard phase ϕ (figure 4*a*–*c*).

The modulus and the strength (figure 4*a*,*b*) of all materials cover a wide range of values within the theoretical bounds [30–32], demonstrating the thoroughness of our exploration. In terms of energy absorption (figure 4*c*), the vast majority of the materials fell within an envelope defined by the rule of mixture ($U/U_s = 1 - \phi$). In general, materials from the 'very brittle' group displayed the highest modulus and strength, but no energy absorption. On the other hand, the ductile weak materials displayed the lowest modulus, lowest strength but highest

energy dissipation. Material from the two intermediate groups fell within these two extremes, except for energy, where some of the 'quasi-brittle' and 'strong ductile' materials exceeded the rule of mixture by a large margin (these particular structures will be discussed later in the article). Our results confirm that while stiffness and strength usually come together (figure 4*d*), strength and toughness are generally mutually exclusive properties (figure 4*e*). The exhaustive search, therefore, provides a powerful tool for parametric studies. Global trends between properties can be identified, the envelopes of possible combinations of properties given a set of hard and soft materials can be assessed, and general structure–properties connection can be established. A very attractive outcome of this approach is also the identification of the most appropriate microstructure for a desired set of properties.

4. Optimum microstructures

The exhaustive explorations can also be used to identify optimum microstructures for a set of desired properties.

Figure 5. Ternary diagrams displaying the best materials as functions of m, n and k and for (a) strong contrast between hard and soft and (b) weak contrast. The colour bar corresponds to the volume fraction of the hard phase. (Online version in colour.)

In contrast with traditional optimization schemes which optimize structures from a pre-determined objective function, here we simply select the 'best' designs from the massive set of data generated over the exhaustive exploration (figure 1). The term 'best' must however be carefully defined, because the best microstructure for stiffness or strength will probably be different from the best structure for toughness. In fact, in many cases, a combination of these three properties may be desired. It is therefore useful to define an index which would measure how well a particular microstructure is adapted to a set of desired properties. Here, we defined a non-dimensional fitness score for the material as

$$f = \left(\frac{E}{E_s}\right)^m \left(\frac{\sigma}{\sigma_s}\right)^n \left(\frac{U}{U_s}\right)^k \quad \text{with} \quad m+n+k=1. \quad (4.1)$$

The indices m, n and k can be continuously adjusted depending on the combination of properties desired for a specific function. For example, $(m,n,k) = (0.1,0.1,0.8)$ may be chosen if energy dissipation is preferred over strength and stiffness. Note that because each of the properties is normalized by the properties of the soft material, $f = 1$ for pure soft material, and for any value of m, n and k. The score f may therefore be interpreted as the improvement achieved by incorporating hard inclusions into a soft matrix. Once a set of desired combinations of properties (m,n,k) has been chosen, it is then easy to identify from the pool of data, collected from the exhaustive exploration of the different microstructures, which is the fittest to achieve this combination, i.e. with the highest index f. Furthermore, in order to keep the results general and to give an overview of the process, we have displayed the best microstructures for *any* combination of m, n and k. Since the sum of the indices is one, the 'fittest' designs can be conveniently displayed in ternary diagrams, as shown in figure 5 for two different levels of contrast between hard and soft phases. These diagrams can be easily constructed from the results of

the exhaustive search. By contrast, constructing this diagram from objective function-based topology optimization methods would require performing an optimization for every combination of m, n and k. The results show that particular optimum designs can occupy large sectors in the diagrams, corresponding in some cases to a wide range of values for (m,n,k). The overall structure of the diagram confirms that designs which offer a certain amount of strength usually offer a similar amount of stiffness: the sectors are broadly organized over horizontal lines of constant k value. Another consistent trend is the concentration of the hard phase: relatively low when energy absorption is favoured (top of the diagram), the concentration of hard phase consistently increases across all designs when more strength and stiffness are required. Pure hard phase is the best material when only strength and stiffness matter ($k = 0$). When only a small amount of energy absorption is needed ($0 < k < 0.1$), the soft phase has very low concentration and appears only as small inclusions in a hard matrix. More sophisticated morphologies emerge when combinations of E, σ and U are desired. The familiar staggered structure emerges as the fittest for regions $k > 0.1$ for both weak and strong contrasts. In this structure, the hard phase comes in the form of inclusions elongated along the direction of loading, and staggered as to form a 'brick-wall'-like structure, the soft phase serving as 'mortar' between the inclusions. For strong contrast between hard and soft phases ($E_h/E_s = 100$, $\sigma_h/\sigma_s = 100$), the staggered structure dominates the diagram, up to $k = 0.7$ (figure 5a). This particular microstructure is found in a wide variety of natural materials which combine soft and hard materials including nacre from mollusc shells, bone, teeth and spider silk [20–24]. These hybrids combine materials with high contrast of properties: soft biological polymers (amorphous proteins and polysaccharides) with hard inclusions (biominerals and crystalized proteins).

When high stiffness and high strength are desired over energy absorption the mineral concentration is high, and the inclusions largely overlap. As more energy dissipation is needed (increasing k), the concentration of mineral diminishes, as more soft material is added between the inclusions. Larger volume fractions of the soft phase generate more energy dissipation per unit volume. For $k > 0.7$ (high energy absorption needed), the familiar layered structure (Reuss composite) emerges as the best design. This particular design is used in engineering laminated composite and also in natural materials such as arthropod cuticles [22,30]. The dactyl of stomatopods (mantis shrimps) represents an extreme example of this type of structure, which is capable of absorbing tremendous impact energies [33].

In the case of weaker contrast between hard and soft ($E_h/E_s = 10$, $\sigma_h/\sigma_s = 10$), the diagram is dominated by the layered structure, while the staggered structure is much less prominent. In this case, the staggered structure appears only when strength with some energy absorption is needed, and with very short inclusions. When the hard phase is not sufficiently strong only short inclusions can be used as longer inclusions would fail prematurely. When higher modulus and/or energy absorption are needed, the layered structure becomes more advantageous. Interestingly, the region $k > 0.7$ is dominated by pure soft material: when high energy dissipation is needed and the reinforcing phase has low contrast of properties with the soft phase, it is more beneficial not to add any reinforcing phase at all. We hypothesize that decreasing the contrast between hard and soft further would lead to diagrams increasingly dominated by pure soft phase, with the extreme case of no contrast between the two phase, in which case it is never advantageous to add a hard phase. The ternary diagram is also revealing for what it does *not* show: for example, continuous reinforcements along the direction of loading, a popular design in composite materials, is completely absent from the list of best designs. Composites with low concentration of small and hard inclusions are also absent from the optimum designs.

5. Concluding remarks

Hybrid materials are a powerful approach in achieving unusual and attractive sets of properties for biological and engineering materials. The question of how to arrange different materials to achieve a given set of hybrid properties is central for the optimization of this class of materials. Traditional optimization methods lead to interesting solutions, but constraints must be placed on the design space and special precautions must be taken to avoid finding a local optimum point. Similarly, natural materials may inspire new hybrid designs, but there is no evidence that nature always uses the best possible structures. This study demonstrates how a simple model and an exhaustive exploration can provide a formidable tool to assess and compare optimum hybrid designs. The process can also be used as a large-scale parametric study, yielding a thorough understanding of structure–properties relationships. Because there is no pre-determined objective function during the exploration, the best designs can be easily identified for any set or range of properties. Today's computer power and parallelization capabilities make this simple approach attractive over existing optimization strategies: an exhaustive search not only guarantees that the optimum design is identified, but also suggests new designs and provides a broad picture of the design space. The results of the exhaustive search may also serve as starting point to more traditional topology optimization schemes which could be used to refine particular designs. The approach presented here can also be extended to explore more sophisticated structural and mechanical features. For example, our models only considered failure of the hard or the soft phase. Debonding between the hard and soft phases could also be introduced and modelled, for example, with cohesive elements [34,35]. Other features such as anisotropy, heterogeneities or even functionally graded properties may be introduced and modelled in the hard and soft phases, these features being present in natural materials. Finally, the structures found in natural material are typically organized over several distinct length scales, and this structural hierarchy further increases their mechanical performance [12,36,37]. This work focused on structures at a single length scale and no exact length scale was associated with the models. Our approach can however also be extended to systematically explore hierarchical structures [38], in order to unveil and exploit synergies of mechanisms at different length scales.

References

1. Ashby MF, Bréchet YJM. 2003 Designing hybrid materials. *Acta Mater.* **51**, 5801–5821. (doi:10.1016/S1359-6454(03)00441-5)

2. Ashby MF. 2005 Hybrids to fill holes in material property space. *Philos. Mag.* **85**, 3235–3257. (doi:10.1080/14786430500079892)

3. Espinosa HD, Rim JE, Barthelat F, Buehler MJ. 2009 Merger of structure and material in nacre and bone—perspectives on de novo biomimetic materials. *Progr. Mater. Sci.* **54**, 1059–1100. (doi:10.1016/j.pmatsci.2009.05.001)

4. Ritchie RO. 2011 The conflicts between strength and toughness. *Nat. Mater.* **10**, 817–822. (doi:10.1038/nmat3115)

5. Zok FW, Waltner SA, Wei Z, Rathbun HJ, McMeeking RM, Evans AG. 2004 A protocol for characterizing the structural performance of metallic sandwich panels: application to pyramidal truss cores. *Int. J. Solids Struct.* **41**, 6249–6271. (doi:10.1016/j.ijsolstr.2004.05.045)

6. Aceves CM, Skordos AA, Sutcliffe MPF. 2008 Design selection methodology for composite structures. *Mater. Des.* **29**, 418–426. (doi:10.1016/j.matdes.2007.01.014)

7. Aceves CM, Sutcliffe MPF, Ashby MF, Skordos AA, Rodriguez Roman C. 2012 Design methodology for composite structures: a small low air-speed wind turbine blade case study. *Mater. Des.* **36**, 296–305. (doi:10.1016/j.matdes.2011.11.033)

8. Bendsoe MP, Sigmund O. 1999 Material interpolation schemes in topology optimization. *Arch. Appl. Mech.* **69**, 635–654. (doi:10.1007/s004190050248)

9. Guo X, Gao H. 2006 Bio-inspired material design and optimization. In *IUTAM Symp. on Topological Design Optimization of Structures, Machines and Materials,* vol. 137 (eds MP Bendsoe, N Olhoff, O Sigmund), pp. 439–453. The Netherlands: Springer.

10. Huang X, Zhou SW, Xie YM, Li Q. 2013 Topology optimization of microstructures of cellular materials and composites for macrostructures. *Comput. Mater. Sci.* **67**, 397–407. (doi:10.1016/j.commatsci.2012.09.018)

11. Torquato S. 2010 Optimal design of heterogeneous materials. In *Annual review of materials research,* vol. 40 (eds DR Clarke, M Ruhle, F Zok), pp. 101–129. Princeton, NJ: Princeton University.

12. Gao HJ. 2006 Application of fracture mechanics concepts to hierarchical biomechanics of bone and bone-like materials. *Int. J. Fract.* **138**, 101–137. (doi:10.1007/s10704-006-7156-4)

13. Maute K, Schwarz S, Ramm E. 1998 Adaptive topology optimization of elastoplastic structures. *Struct. Optim.* **15**, 81–91. (doi:10.1007/BF01278493)

14. Sigmund O. 2000 A new class of extremal composites. *J. Mech. Phys. Solids* **48**, 397–428. (doi:10.1016/S0022-5096(99)00034-4)

15. Torquato S. 2000 Modeling of physical properties of composite materials. *Int. J. Solids Struct.* **37**, 411–422. (doi:10.1016/S0020-7683(99)00103-1)

16. Torquato S, Hyun S, Donev A. 2002 Multifunctional composites: optimizing microstructures for simultaneous transport of heat and electricity. *Phys. Rev. Lett.* **89**, 266601. (doi:10.1103/PhysRevLett.89.266601)

17. Sigmund O, Petersson J. 1998 Numerical instabilities in topology optimization: a survey on procedures dealing with checkerboards, mesh-dependencies and local minima. *Struct. Optim.* **16**, 68–75. (doi:10.1007/BF01214002)

18. Liang QQ. 2007 Performance-based optimization: a review. *Adv. Struct. Eng.* **10**, 739–753. (doi:10.1260/136943307783571418)

19. Nievergelt J. 2000 Exhaustive search, combinatorial optimization and enumeration: exploring the potential of raw computing power. In *Sofsem 2000: theory and practice of informatics* (eds V Hlavac, KG Jeffery, J Wiedermann), pp. 18–35. Lecture Notes in Computer Science. Berlin, Germany: Springer.

20. Meyers MA, Chen PY, Lin AYM, Seki Y. 2008 Biological materials: structure and mechanical properties. *Progr. Mater. Sci.* **53**, 1–206. (doi:10.1016/j.pmatsci.2007.05.002)

21. Barthelat F. 2007 Biomimetics for next generation materials. *Phil. Trans. R. Soc. A* **365**, 2907–2919. (doi:10.1098/rsta.2007.0006)

22. Hackman R, Goldberg M. 1987 Comparative study of some expanding arthropod cuticles: the relation between composition, structure and function. *J. Insect Physiol.* **33**, 39–50. (doi:10.1016/0022-1910(87)90102-8)

23. He LH, Swain MV. 2008 Understanding the mechanical behaviour of human enamel from its structural and compositional characteristics. *J. Mech. Behav. Biomed. Mater.* **1**, 18–29. (doi:10.1016/j.jmbbm.2007.05.001)

24. Zhu D, Ortega CF, Motamedi R, Szewciw L, Vernerey F, Barthelat F. 2012 Structure and mechanical performance of a 'modern' fish scale. *Adv. Eng. Mater.* **14**, B185–B194. (doi:10.1002/adem.201180057)

25. Barthelat F, Tang H, Zavattieri PD, Li CM, Espinosa HD. 2007 On the mechanics of mother-of-pearl: a key feature in the material hierarchical structure. *J. Mech. Phys. Solids* **55**, 225–444. (doi:10.1016/j.jmps.2006.07.007)

26. Asmani M, Kermel C, Leriche A, Ourak M. 2001 Influence of porosity on Young's modulus and Poisson's ratio in alumina ceramics. *J. Eur. Ceram. Soc.* **21**, 1081–1086. (doi:10.1016/S0955-2219(00)00314-9)

27. Tschoegl NW, Knauss WG, Emri I. 2002 Poisson's ratio in linear viscoelasticity: a critical review. *Mech. Time-Depend. Mater.* **6**, 3–51. (doi:10.1023/A:1014411503170)

28. Seltzer R, Cisilino AP, Frontini PM, Mai YW. 2011 Determination of the Drucker–Prager parameters of polymers exhibiting pressure-sensitive plastic behaviour by depth-sensing indentation. *Int. J. Mech. Sci.* **53**, 471–478. (doi:10.1016/j.ijmecsci.2011.04.002)

29. Dean G, Crocker L, Read B, Wright L. 2004 Prediction of deformation and failure of rubber-toughened adhesive joints. *Int. J. Adhes. Adhes.* **24**, 295–306. (doi:10.1016/j.ijadhadh.2003.08.002)

30. Reuss A. 1929 Berechnung der fließgrenze von mischkristallen auf grund den konstanten des einkristalls. *Z. Angew. Math. Mech.* **9**, 49–58. (doi:10.1002/zamm.19290090104)

31. Voigt W. 1928 *Lehrbuch der Kristallphysik*. Leipzig, Germany: Teubner.

32. Martin JW. 2006 *Concise encyclopedia of the structure of materials*. Amsterdam, The Netherlands: Elsevier Science.

33. Weaver JC et al. 2012 The stomatopod dactyl club: a formidable damage-tolerant biological hammer. *Science* **336**, 1275–1280. (doi:10.1126/science.1218764)

34. Khayer Dastjerdi A, Pagano M, Kaartinen M, McKee M, Barthelat F. 2012 The cohesive behavior of soft biological 'glues': experiments and modeling. *Acta Biomater.* **8**, 3349–3359. (doi:10.1016/j.actbio.2012.05.005)

35. Rabiei R, Bekah S, Barthelat F. 2010 Failure mode transition in nacre and bone-like materials. *Acta Biomater.* **6**, 4081–4089. (doi:10.1016/j.actbio.2010.04.008)

36. Bechtle S, Ang SF, Schneider GA. 2010 On the mechanical properties of hierarchically structured biological materials. *Biomaterials* **31**, 6378–6385. (doi:10.1016/j.biomaterials.2010.05.044)

37. Sen D, Buehler MJ. 2011 Structural hierarchies define toughness and defect-tolerance despite simple and mechanically inferior brittle building blocks. *Sci. Rep.* **1**, 35. (doi:10.1038/srep00035)

38. Zhang Z, Zhang YW, Gao H. 2011 On optimal hierarchy of load-bearing biological materials. *Proc. R. Soc. B* **278**, 519–525. (doi:10.1098/rspb.2010.1093)